


 Cite this: *Nanoscale*, 2023, **15**, 7710

Received 7th December 2022,

Accepted 30th January 2023

DOI: 10.1039/d2nr06840k

[rsc.li/nanoscale](https://rsc.li/nanoscale)

## Investigating the interfacial properties of halide perovskite/TiO<sub>x</sub> heterostructures for versatile photocatalytic reactions under sunlight†

 Tae Hyung Kim,<sup>a</sup> Inho Park,<sup>a</sup> Kyeong Ho Lee,<sup>a</sup> Jin-Han Sim,<sup>b</sup> Min-Ho Park,<sup>c</sup> Tae-Hee Han,<sup>b</sup> Ungyu Paik,<sup>id</sup> <sup>a</sup> Jaeyoung Jang,<sup>id</sup> <sup>\*a</sup> Ho Bum Park<sup>id</sup> <sup>\*a</sup> and Young-Hoon Kim<sup>id</sup> <sup>\*a</sup>

Heterostructures of metal halide perovskites and TiO<sub>x</sub> are efficient photocatalytic materials owing to the combination of the advantages of each compound, specifically the high absorption coefficients and long charge-carrier lifetimes of perovskites, and efficient photocatalytic activity of TiO<sub>x</sub>. However, chemical reduction of CO<sub>2</sub> using PNC/TiO<sub>x</sub> heterostructures without organic solvents has not been reported yet. Here, we report the first solvent-free reduction of CO<sub>2</sub> using amorphous TiO<sub>x</sub> with embedded colloidal perovskite nanocrystals (PNCs). The combination was obtained by carrying out hydrolysis of titanium butoxide (TBOT) on the PNC surface without high-temperature calcination. We proposed a mechanism involving photoexcited electrons being transferred from PNCs to TBOT, enabling photocatalytic reactions using TiO<sub>x</sub> under visible-light excitation. We demonstrated efficient visible-light-driven photocatalytic reactions at PNC/TiO<sub>x</sub> interfaces, specifically with a CO production rate of 30.43 μmol g<sup>-1</sup> h<sup>-1</sup> and accelerated degradation of organic pollutants under natural sunlight. Our work has provided a simple path toward both efficient CO<sub>2</sub> reduction and photocatalytic degradation of organic dyes.

### Introduction

As human civilization went through the industrial revolution and the population has increased, our world faces serious global crises, especially global warming<sup>1</sup> and water pollution, both of which threaten the environment and human civiliza-

tion. Various strategies for decreasing CO<sub>2</sub> emissions and water pollutants have been attempted: biological,<sup>2</sup> electrochemical,<sup>3</sup> photochemical<sup>4</sup> and photoelectrochemical<sup>5</sup> conversion techniques have been tested for converting CO<sub>2</sub> to valuable chemicals and fuels; and biodegradation,<sup>6</sup> electrochemical oxidation<sup>7</sup> and photocatalytic reduction<sup>8</sup> have been applied to eliminate dye contaminations. Of these strategies, use of photocatalysts is considered the most promising one for decreasing both atmospheric CO<sub>2</sub> gas and organic pollutants because photocatalysts have wide applicability and can degrade organic materials to harmless products such as H<sub>2</sub>O and H<sub>2</sub>. This ability can be exploited to reduce CO<sub>2</sub> emission and degrade water pollutants. The process can be also powered by sunlight, which is free and essentially infinite. Photochemical reactions to decrease the amounts of CO<sub>2</sub> or water pollutants have been achieved using various materials such as metal oxides (*e.g.*, TiO<sub>2</sub>, Cu<sub>2</sub>O, WO<sub>3</sub>, Bi<sub>2</sub>WO<sub>6</sub>, Zn<sub>2</sub>GeO<sub>4</sub>, ZnGa<sub>2</sub>O<sub>4</sub>, oxide perovskites),<sup>9–11</sup> metal-organic frameworks,<sup>12</sup> nitrides (*e.g.*, C<sub>3</sub>N<sub>4</sub>, GaN, (Zn<sub>1+x</sub>Ge)(N<sub>2</sub>O<sub>x</sub>)),<sup>13</sup> sulfides (*e.g.*, CdS, ZnS and Cu<sub>2</sub>ZnSnS<sub>4</sub>),<sup>14</sup> and phosphides (*e.g.*, InP, GaP).<sup>15</sup> However, these materials have wide bandgaps (for instance, >3.2 eV for TiO<sub>2</sub>,<sup>16</sup> and >3.25 eV for WO<sub>3</sub><sup>17</sup>), so they initiate catalytic reactions only under ultraviolet (UV) light (wavelength λ < 400 nm). However, only less than 5% of sunlight has photons in these wavelengths, so photocatalytic reactions in conventional photocatalytic materials require an additional UV source. Also, in these conventional materials, recombination of charge carriers is rapid, so the photocatalytic reaction efficiency is relatively poor. Therefore, efficient chemical reduction of CO<sub>2</sub> and degradation of organic pollutants under sunlight require new materials that use wavelengths >400 nm, have high absorption coefficients, and show slow recombination of charge carriers and efficient photocatalytic reaction capabilities.

To achieve these goals, heterostructures in which an “absorber” traps light and transfers excited electrons to a “photocatalyst” have been tested. Halide perovskites have been regarded as promising light absorbers due to their high absorption coefficients, long carrier diffusion paths, long

<sup>a</sup>Department of Energy Engineering, Hanyang University, 222 Wangsimni-ro, Seongdong-gu, Seoul 04763, Republic of Korea. E-mail: [jjyang15@hanyang.ac.kr](mailto:jjyang15@hanyang.ac.kr), [badtzhb@hanyang.ac.kr](mailto:badtzhb@hanyang.ac.kr), [younghoonkim@hanyang.ac.kr](mailto:younghoonkim@hanyang.ac.kr)

<sup>b</sup>Division of Materials Science and Engineering, 222 Wangsimni-ro, Seongdong-gu, Seoul 04763, Republic of Korea

<sup>c</sup>Department of Materials Science and Engineering, Department of Green Chemistry and Materials Engineering, Soongsil University, 369 Sangdo-Ro, Dongjak-Gu, Seoul 06978, Republic of Korea

† Electronic supplementary information (ESI) available. See DOI: <https://doi.org/10.1039/d2nr06840k>

charge carrier lifetimes and tunable bandgaps.<sup>18,19</sup> Amorphous  $\text{TiO}_x$  ( $\text{TiO}_x$ ) or crystalline  $\text{TiO}_2$  are efficient photocatalysts due to their electrical conductivity, decent photocatalytic activity and excellent chemical stability levels.<sup>20</sup>

Halide perovskite nanocrystals (PNCs) embedded in  $\text{TiO}_x$  matrices<sup>21</sup> or in  $\text{TiO}_2$  nanofibers<sup>22</sup> have been developed to facilitate chemical reduction of  $\text{CO}_2$  by virtue of the photo-induced excitation of charges in the PNCs and transfer and extraction of these excited charges to  $\text{TiO}_x$ . These reactions are generally carried out with an external power supply (under Xe-lamp irradiation, which covers the ultraviolet-visible light range ( $100 \text{ nm} < \lambda \leq 800 \text{ nm}$ )), with the  $\text{CO}_2$  reduction rates measured in the presence of organic solvents (ethyl acetate,<sup>21</sup> acetonitrile<sup>22</sup>). Natural sunlight, which is an essentially infinite resource, can be utilized to realize the photocatalytic reactions, which would decrease both  $\text{CO}_2$  emissions and generation of water pollutants without use of an additional external power consumption. To the best of our knowledge, the chemical reduction of  $\text{CO}_2$  using PNC/ $\text{TiO}_x$  (or  $\text{TiO}_2$ ) heterostructures under sunlight illumination has not been reported. Moreover, perovskite-photocatalyzed reduction of  $\text{CO}_2$  is often overestimated in  $\text{CO}_2$  reduction experiments that are conducted in the presence of organic solvents because the organic solvents can be transformed (at a rate of, for example,  $\sim 1 \text{ mmol g}^{-1} \text{ h}^{-1}$ ) into reduced products such as  $\text{CO}$  and  $\text{CH}_4$ .<sup>23</sup> So far,  $\text{CO}_2$  reduction using PNC/ $\text{TiO}_x$  heterostructures without organic solvents has not been reported.

Here we developed a reduction of  $\text{CO}_2$  not involving the use of an organic solvent by using PNC/ $\text{TiO}_x$  heterostructures in which the PNCs absorbed visible sunlight and boosted the photocatalytic reactions at the  $\text{TiO}_x$  component.  $\text{TiO}_x$  formed on the surfaces of  $\text{CsPbBr}_3$  PNCs as a result of hydrolysis of titanium butoxide (TBOT) without high-temperature calcination. We proposed a mechanism involving transfer of photo-excited electrons to TBOT, allowing for the first solvent-free  $\text{CO}_2$  reduction based on PNC/ $\text{TiO}_x$  heterostructures. PNC/ $\text{TiO}_x$  heterostructures decreased  $\text{CO}_2$  concentration at a rate of  $30.43 \mu\text{mol g}^{-1} \text{ h}^{-1}$  under outdoor sunlight without use of any other external energy. Moreover, we demonstrated more efficient degradation of organic dye under visible white light ( $\lambda = 400 \text{ nm}$ – $780 \text{ nm}$ ), green light ( $\lambda = 500$ – $520 \text{ nm}$ ) and outdoor sunlight by PNC/ $\text{TiO}_x$  heterostructures than by pure PNCs and  $\text{TiO}_x$ .

## Results and discussion

### Synthesis of PNC/ $\text{TiO}_x$ heterostructures

PNC/ $\text{TiO}_x$  heterostructures were synthesized by introducing and then hydrolyzing TBOT ( $\text{O-Ti}(\text{OC}_4\text{H}_9)_4$ ) on the surface of pre-synthesized  $\text{CsPbBr}_3$  PNCs (Fig. 1a). Before synthesis of the heterostructures, the PNCs were cubic with an average size of  $9.4 \text{ nm}$ , and showed a peak at  $511.1 \text{ nm}$  in the PL spectrum, with an FWHM of  $20 \text{ nm}$  (Fig. S1a and b†). After injection of TBOT, the PNC solutions showed a significant decrease in PL intensity with a sudden redshift of the peak in the PL spec-

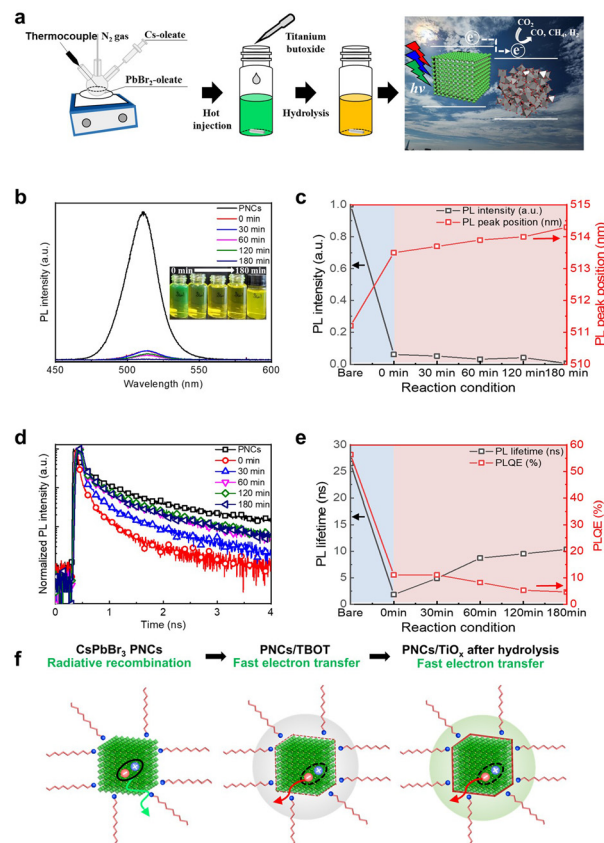


**Fig. 1** (a) Schematic illustrations of the introduction of TBOT into  $\text{CsPbBr}_3$  PNCs (left), subsequent hydrolysis of TBOT (middle), and photocatalytic reactions of  $\text{CsPbBr}_3/\text{TiO}_x$  heterostructures under sunlight (right). (b) PL spectrum (inset: optical images of solutions), (c) PL intensity and PL peak wavelength as a function of reaction time, (d) time-resolved PL spectra, (e) PL lifetime and PLQE and (f) schematic illustrations of charge carrier behaviors for formation of  $\text{CsPbBr}_3/\text{TiO}_x$  heterostructures under continuous hydrolysis.

trum from  $511.1 \text{ nm}$  to  $514.3 \text{ nm}$ , attributed to TBOT having adhered to the surfaces of the PNCs and inducing severe exciton dissociation in them (Fig. 1b and c). As the TBOT was hydrolyzed in air with 40% humidity, composite solutions showed a gradual change of color from bright green to turbid yellow (Fig. 1b, inset), and a gradual decrease of PL intensity with a redshift of the PL signal (Fig. 1c, and S2†).

### Photophysical properties

To quantify the charge carrier dynamics in the composites, we measured PL lifetimes, and did so by conducting time-correlated single-photon counting (TCSPC) with excitation laser irradiation (wavelength =  $405 \text{ nm}$ ) of the composite solutions. After injection of TBOT into  $\text{CsPbBr}_3$  PNCs, the heterostructures showed dramatically decreased  $\tau_{\text{ave}}$  (from  $\tau_{\text{ave}}$  of  $26.51 \text{ ns}$  for  $\text{CsPbBr}_3$  PNCs to  $\tau_{\text{ave}}$  of  $1.8 \text{ ns}$  for  $\text{CsPbBr}_3/\text{TBOT}$  composites) due to exciton quenching and electron transfer by TBOT on the PNC surfaces (Fig. 1d, e, and Table S1†). This result corresponded well to the observed sudden decrease in PL intensity (Fig. 1b and c). After the initial rapid decrease in

PL lifetime upon addition of TBOT, the composite solutions showed gradually increasing  $\tau_{\text{ave}}$  ( $\tau_{\text{ave}} = 10.33$  ns, heterostructures with 180 minutes of reaction). These increases in the PL lifetime were opposite the decrease in the PL intensity (Fig. 1c, d, and S2†). We attributed the increase in PL lifetime upon hydrolysis of TBOT to the aggregation of nanoparticles (Fig. S3–6†).

Using measured average PL lifetimes, we investigated the rate of electron transfer  $k_{\text{ET}}$  from PNCs to TBOT. The  $k_{\text{ET}}$  parameter was derived using the equation<sup>24</sup>

$$k_{\text{ET}} = \frac{1}{\tau_{\text{CsPbBr}_3/\text{TBOT}}} - \frac{1}{\tau_{\text{CsPbBr}_3}} \quad (1)$$

where  $\tau_{\text{CsPbBr}_3/\text{TBOT}}$  and  $\tau_{\text{CsPbBr}_3}$  are the PL lifetimes of the CsPbBr<sub>3</sub>/TBOT composites and CsPbBr<sub>3</sub> PNC, respectively. And  $k_{\text{ET}}$  of CsPbBr<sub>3</sub>/TBOT was calculated to be  $5.18 \times 10^8$ , a value 5 times that of the previously reported CsPbBr<sub>3</sub>/TiO<sub>2</sub> ( $k_{\text{ET}} = 9.7 \times 10^7$  s<sup>-1</sup>),<sup>24</sup> indicative of efficient charge transfer at the CsPbBr<sub>3</sub>/TBOT interface.

### Chemical and structural properties

To study the chemical properties of the heterostructure surfaces upon hydrolysis of TBOT, we performed FTIR spectroscopy experiments (Fig. S7a and b†). When TBOT was introduced to the PNC solutions, increases were observed in the intensities of the C–H signals of O–Ti(OC<sub>4</sub>H<sub>9</sub>)<sub>4</sub> at 3430 cm<sup>-1</sup>, the COO<sup>-</sup> and CH<sub>3</sub> signals at 1468–1380 cm<sup>-1</sup>, the C–H stretching signals at 2923–2854 cm<sup>-1</sup> (Fig. S7a†) and the Ti–O–C bond signals at 1125–1035 cm<sup>-1</sup> (Fig. S7b†). As the hydrolysis proceeded, the intensities of these signals decreased linearly; this trend confirmed that TBOT became converted to TiO<sub>x</sub> as suggested in the PL and time-resolved PL spectra analysis. When the hydrolysis reaction had finished (180 minutes after initiation of hydrolysis when the PL lifetime, intensity and spectrum stopped changing), heterostructures were collected by performing sequential centrifugation and dried by performing evaporation of residual solvent in vacuum.

Then we determined the crystal structure of CsPbBr<sub>3</sub>/TiO<sub>x</sub> heterostructures by conducting X-ray diffraction (XRD) spectroscopy (Fig. 2a). The heterostructures yielded clear XRD peaks at 15.1°, 21.1°, 29.8°, 29.9°, 34.7°, 36.9° and 44.6°, which corresponded to (100), (110), (004), (200), (210), (211) and (220) crystal planes, respectively; these observations were consistent with peaks of CsPbBr<sub>3</sub> PNCs. Amorphous TiO<sub>x</sub> without PNCs did not show any clear XRD peaks. High-resolution TEM showed PNCs embedded in the TiO<sub>x</sub> matrix with clear lattice constants of 3.0 and 4.1 Å, which corresponded to, respectively, (002) and (110) planes in the CsPbBr<sub>3</sub> PNCs (Fig. S8†). To study the chemical formation and electrical interaction at the interfaces in the heterostructures, we collected X-ray photoelectron spectroscopy (XPS) data from control TiO<sub>x</sub>, PNCs and the heterostructures (Fig. 2b–d, and S9†). The heterostructures showed XPS peaks assigned to Br (~68.0 eV), Pb (~137.9 and 143.0 eV) and Ti (~464.2 eV, 458.2 eV), which indicated the presence of both CsPbBr<sub>3</sub> and TiO<sub>x</sub>.

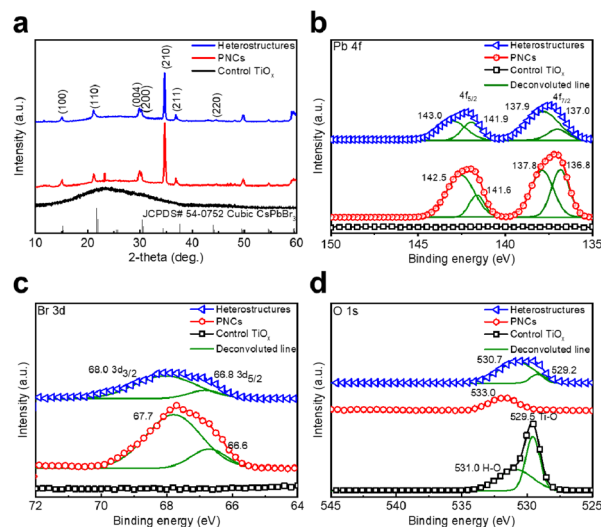
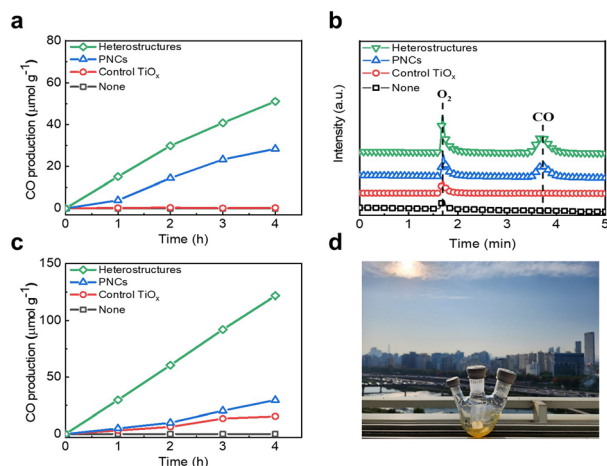


Fig. 2 (a) XRD patterns and (b) Pb 4f, (c) Br 3d and (d) O 1s regions of the XPS spectra of the CsPbBr<sub>3</sub>/TiO<sub>x</sub> heterostructures, PNCs and control TiO<sub>x</sub>.

Signals of Pb and Br from CsPbBr<sub>3</sub> in the heterostructures were blue-shifted toward higher binding energy compared to those in PNCs (from ~142.5 eV for 4f<sub>5/2</sub>, ~137.8 eV for 4f<sub>7/2</sub>, ~67.7 eV for 3d<sub>3/2</sub>, ~66.6 eV for 3d<sub>5/2</sub> in PNCs to ~143.0 eV for 4f<sub>5/2</sub>, ~137.9 eV for 4f<sub>7/2</sub>, ~68.0 eV for 3d<sub>3/2</sub>, ~66.8 eV for 3d<sub>5/2</sub> in heterostructures). These XPS peak shifts indicated that electron transfers from CsPbBr<sub>3</sub> to TiO<sub>x</sub> occurred at the interface, in turn attributed to a shallower conduction band minimum (CBM) of CsPbBr<sub>3</sub> (~-3.9 eV)<sup>25</sup> than of TiO<sub>x</sub> (~-4.00 eV).<sup>26</sup> This transfer focused the electrons towards TiO<sub>x</sub> and boosted the photocatalytic activity of TiO<sub>x</sub>.

### Photocatalytic reactions

To evaluate the photocatalytic activities of the heterostructures, we conducted photochemical CO<sub>2</sub> conversion analysis of control TiO<sub>x</sub>, PNCs and the heterostructures (results summarized in Table S2†). To prevent side reactions and enable correct measurement of the CO<sub>2</sub> conversion efficiencies of our samples, the light intensity was measured during the reaction (Fig. S10 and Table S3†) and the experiments were performed in a gas–solid reaction system without any sacrificial reagents or organic solvents.<sup>23</sup> First, an external light source was tested for practical analysis. Under visible white light irradiation (400 ≤ λ ≤ 780 nm, Fig. S10†), CsPbBr<sub>3</sub>/TiO<sub>x</sub> heterostructures showed a CO production rate of 12.77 μmol g<sup>-1</sup> h<sup>-1</sup> and photoelectron consumption rate of 25.54 μmol g<sup>-1</sup> h<sup>-1</sup> (Fig. 3a and b). The CO<sub>2</sub> was reduced to CO by consuming two electrons, and no other gasses such as H<sub>2</sub> were detected. PNCs showed a CO production rate of 7.1 μmol g<sup>-1</sup> h<sup>-1</sup>, a value lower than that of the heterostructures, and control TiO<sub>x</sub> did not show any CO production, attributed to the inability of TiO<sub>x</sub> with its wide bandgap (~4 eV) to absorb visible light (400 ≤ λ ≤ 780 nm). Furthermore, control TiO<sub>x</sub>, PNCs and CsPbBr<sub>3</sub>/TiO<sub>x</sub>



**Fig. 3** (a) CO-production rates and (b) GC chromatograms of a sample without any photocatalytic materials ("none"), control TiO<sub>x</sub>, PNCs and heterostructures in white-light illumination, (c) CO-production rates and (d) photograph of CO<sub>2</sub> reduction experiment of heterostructures under outdoor natural sunlight.

heterostructures showed CO production rates of 3.87, 7.44 and 30.43 μmol g<sup>-1</sup> h<sup>-1</sup>, respectively, under natural sunlight without any additional light source such as an Xe lamp or LED light (Fig. 3c and d). To the best of our knowledge, this was the first reported example of a perovskite/TiO<sub>x</sub>-heterostructure-based reduction of CO<sub>2</sub> carried out without using organic solvent.

To further investigate the photocatalytic activities of the heterostructures, we conducted a photocatalytic degradation of orange-light-emitting PPV copolymer (Merck Orange) under white light (400 ≤ λ ≤ 780 nm), green light (450 ≤ λ ≤ 600 nm) and outdoor natural sunlight. The degradations were monitored by tracking maximum absorbance (Fig. S12 and S13<sup>†</sup>), observing the solution color with the naked eye, and FTIR spectroscopy (Fig. S14<sup>†</sup>). The dye degraded much more rapidly in the solution with heterostructures than with control TiO<sub>x</sub> and without any catalytic materials: degradation rates of 77.1% with heterostructures, 62% with control TiO<sub>x</sub> and 18% without any photocatalytic reactors for 9 hours (h) under white light (Fig. 4a, S12a–c<sup>†</sup>); 57% for heterostructures, 47.7% for control TiO<sub>x</sub> and 8.6% for samples without any photocatalytic reactors for 16 h under green light (Fig. S12d–f, and S15<sup>†</sup>); and 86.8% with heterostructures, 65.4% with control TiO<sub>x</sub> and 47.1% with samples without any photocatalytic reactors for 4 h under outdoor sunlight (Fig. 4d, S12g–i<sup>†</sup>). We attributed the degradation of organic dyes with pure TiO<sub>x</sub>, which cannot absorb visible light, to the charge carriers excited in orange PPV copolymer having been transferred to TiO<sub>x</sub> and then inducing the photocatalytic reaction.<sup>27</sup> All of the degradations of organic dye under light irradiation followed a pseudo-first-order decay according to the equation  $\ln(C/C_0) = kt$ , where  $C_0$  is the initial concentration of organic dye,  $C$  is the concentration of organic dye at reaction time  $t$ , and  $k$  is the absorption coefficient.

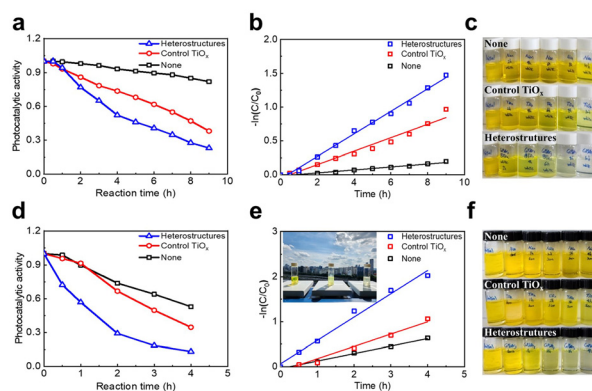


**Fig. 4** (a) Photocatalytic degradation activities, (b) kinetic curves, (c) photographs of PPV copolymer degraded without any photocatalytic materials (top), with control TiO<sub>x</sub> (middle), and with PNC/TiO<sub>x</sub> heterostructures (bottom) under visible white light. (d) Photocatalytic degradation activities, (e) kinetic curves (inset: photograph of experiment) and (f) photographs of PPV copolymer without any photocatalytic materials (top), with control TiO<sub>x</sub> (middle), and with PNC/TiO<sub>x</sub> heterostructures (bottom) under outdoor natural sunlight.

## Conclusions

We have demonstrated an efficient reduction of CO<sub>2</sub> without organic solvent in PNC systems by forming TiO<sub>x</sub> on CsPbBr<sub>3</sub> PNC surfaces as a result of hydrolyzing TBOT without high-temperature calcination. Photoexcited electrons in the resulting heterostructures were concluded to be transferred to TBOT and then TiO<sub>x</sub> upon conversion of the TBOT to TiO<sub>x</sub>, with this transfer slowing the recombination of charge carriers and having achieved in our experiments a solvent-free CO<sub>2</sub> reduction rate of 30.43 μmol g<sup>-1</sup> h<sup>-1</sup> under sunlight. To the best of our knowledge, this was the first reported example of PNC/TiO<sub>x</sub>-heterostructure-based CO<sub>2</sub> reduction without any organic solvent. We also demonstrated that PNC/TiO<sub>x</sub> heterostructures can be used to boost photocatalytic degradation of organic dye under visible white light, green light and outdoor sunlight. This result has suggested the use of halide perovskites as a step towards the development of environmentally benign CO<sub>2</sub> reduction and pollutant reduction.

## Note added after first publication

This article replaces the version published on 31<sup>st</sup> January 2023. Since the first publication, the authors were made aware of a late reviewer's concerns regarding the time-resolved photoluminescence (PL) lifetime data, which the authors and Editorial Office felt it would be best to address. The outcome of this consideration was that the authors re-conducted the experiment and have now attributed the increase in PL lifetime with hydrolysis of TBOT to an artefactual aggregation of nanoparticles during hydrolysis. Minor changes to the text of the main article, including a revision of eqn (1) and removal of eqn (2) in the Results and discussion section, have been made

with the approval of the handling Associate Editor. Changes have also been made to ESI Fig. S3–S6,† most notably the addition of further discussion of the PL lifetimes following Fig. S4.† These changes have been reviewed by the handling Associate Editor and the authors confirm that the main findings of the article have not been significantly altered.

## Conflicts of interest

There are no conflicts to declare.

## Acknowledgements

This work was supported by the research fund of National Research Foundation of Korea (NRF) grant funded by the Korea government (MSIT) (2022R1A5A1032539, 2022R1C1C1008282) and Industrial Strategic Technology Development Program-Alchemist Project (1415180859, Chiral perovskite LED smart contact lens based hyper vision meta-verse) funded by the Ministry of Trade, Industry & Energy (MOTIE, Korea) and Korea Evaluation Institute of Industrial Technology (KEIT, Korea).

## References

- M. Mendez-Galvan, B. Alcantar-Vazquez, G. Diaz, I. A. Ibarra and H. A. Lara-Garcia, *React. Chem. Eng.*, 2021, **6**, 828–838.
- F. Tassi, S. Venturi, J. Cabassi, O. Vaselli, I. Gelli, D. Cinti and F. Capecciacci, *Org. Geochem.*, 2015, **86**, 81–93.
- S. Nitopi, E. Bertheussen, S. B. Scott, X. Liu, A. K. Engstfeld, S. Horch, B. Seger, I. E. L. Stephens, K. Chan, C. Hahn, J. K. Nørskov, T. F. Jaramillo and I. Chorkendorff, *Chem. Rev.*, 2019, **119**, 7610–7672.
- U. Ulmer, T. Dingle, P. N. Duchesne, R. H. Morris, A. Tavasoli, T. Wood and G. A. Ozin, *Nat. Commun.*, 2019, **10**, 3169–3180.
- V. Kumaravel, J. Bartlett and S. C. Pillai, *ACS Energy Lett.*, 2020, **5**, 486–519.
- I. Jambon, S. Thijs, G. Torres-Farradá, F. Rineau, N. Weyens, R. Carleer, P. Samyn and J. Vangronsveld, *Front. Microbiol.*, 2019, **10**, 1892–1904.
- C. A. Martínez-Huitle and S. Ferro, *Chem. Soc. Rev.*, 2006, **35**, 1324–1340.
- C. Lu, P. Zhang, S. Jiang, X. Wu, S. Song, M. Zhu, Z. Lou, Z. Li, F. Liu, Y. Liu, Y. Wang and Z. Le, *Appl. Catal., B*, 2017, **200**, 378–385.
- C. S. Ribeiro, J. Z. Y. Tan, M. M. Maroto-Valer and M. A. Lansarin, *J. Environ. Chem. Eng.*, 2021, **9**, 105097–105106.
- H. Wang, L. Zhang, K. Wang, X. Sun and W. Wang, *Appl. Catal., B*, 2019, **243**, 771–779.
- L. Liu, H. Zhao, J. M. Andino and Y. Li, *ACS Catal.*, 2012, **2**, 1817–1828.
- H. Zhong, M. Ghorbani-Asl, K. H. Ly, J. Zhang, J. Ge, M. Wang, Z. Liao, D. Makarov, E. Zschech, E. Brunner, I. M. Weidinger, J. Zhang, A. v. Krashenninnikov, S. Kaskel, R. Dong and X. Feng, *Nat. Commun.*, 2020, **11**, 1409–1418.
- P. Huang, J. Huang, S. A. Pantovich, A. D. Carl, T. G. Fenton, C. A. Caputo, R. L. Grimm, A. I. Frenkel and G. Li, *J. Am. Chem. Soc.*, 2018, **140**, 16042–16047.
- R. Zhou and M. I. Guzman, *J. Phys. Chem. C*, 2014, **118**, 11649–11656.
- B. Chon, S. Choi, Y. Seo, H. S. Lee, C. H. Kim, H. J. Son and S. O. Kang, *ACS Sustainable Chem. Eng.*, 2022, **10**, 6033–6044.
- C. Dette, M. A. Pérez-Osorio, C. S. Kley, P. Punke, C. E. Patrick, P. Jacobson, F. Giustino, S. J. Jung and K. Kern, *Nano Lett.*, 2014, **14**, 6533–6538.
- R. S. Vemuri, M. H. Engelhard and C. v. Ramana, *ACS Appl. Mater. Interfaces*, 2012, **4**, 1371–1377.
- M. Pawar, S. T. Sendogdular and P. Gouma, *J. Nanomater.*, 2018, **2018**, 5953609–5953621.
- G. Rainò, M. A. Becker, M. I. Bodnarchuk, R. F. Mahrt, M. v. Kovalenko and T. Stöferle, *Nature*, 2018, **563**, 671–675.
- A. Inbal, J. P. Ampuero and R. W. Clayton, *Science*, 2016, **354**, 88–92.
- Y. F. Xu, X. D. Wang, J. F. Liao, B. X. Chen, H. Y. Chen and D. B. Kuang, *Adv. Mater. Interfaces*, 2018, **5**, 1801015–1801022.
- F. Xu, K. Meng, B. Cheng, S. Wang, J. Xu and J. Yu, *Nat. Commun.*, 2020, **11**, 4613–4621.
- J. S. Martin, N. Dang, E. Raulerson, M. C. Beard, J. Hartenberger and Y. Yan, *Angew. Chem., Int. Ed.*, 2022, **61**, e202205572–e202205579.
- X. Liu, H. Zhao, L. Wei, X. Ren, X. Zhang, F. Li, P. Zeng and M. Liu, *Nanophotonics*, 2021, **10**, 1967–1975.
- H. Algadi, C. Mahata, J. Woo, M. Lee, M. Kim and T. Lee, *Electronics*, 2019, **8**, 678–690.
- J. Fujisawa, T. Eda and M. Hanaya, *Chem. Phys. Lett.*, 2017, **685**, 23–26.
- S. A. Kumar, J. S. Shankar and B. K. Periyasamy, *J. Mater. Sci.*, 2022, **57**, 12449–12462.